APPLIED SCIENCES AND ENGINEERING

Biomimetic potassium-selective nanopores

Elif Turker Acar[1,2*†], Steven F. Buchsbaum[3*†], Cody Combs[1], Francesco Fornasiero[3*], Zuzanna S. Siwy[1,4,5*]

Reproducing the exquisite ion selectivity displayed by biological ion channels in artificial nanopore systems has proven to be one of the most challenging tasks undertaken by the nanopore community, yet a successful achievement of this goal offers immense technological potential. Here, we show a strategy to design solid-state nanopores that selectively transport potassium ions and show negligible conductance for sodium ions. The nanopores contain walls decorated with 4′-aminobenzo-18-crown-6 ether and single-stranded DNA (ssDNA) molecules located at one pore entrance. The ionic selectivity stems from facilitated transport of potassium ions in the pore region containing crown ether, while the highly charged ssDNA plays the role of a cation filter. Achieving potassium selectivity in solid-state nanopores opens new avenues toward advanced separation processes, more efficient biosensing technologies, and novel biomimetic nanopore systems.

INTRODUCTION

Since the discovery of biological channels and their importance in physiological processes, scientists have attempted to create robust man-made structures that exhibit transport properties mimicking those of their biological counterparts (*1*–*4*). Responsiveness to external stimuli and exquisite ionic selectivity are two of the most exciting properties for which efficiency remains unmatched by solid-state nanopores (*5*). Stimuli in the form of electrical potential modulation, chemical interactions, or mechanical stress can induce so-called gated channels to switch between ion-conductive and closed states. Biological channels are also frequently able to differentiate between ions of the same charge so that, for example, potassium-selective channels can transport potassium ions thousands of times faster than sodium ions (*6*, *7*). Matching biological gating and ion selectivity capabilities in a synthetic nanopore platform could not only enable new sensing technologies but also lay the groundwork for a deeper understanding of ionic and molecular transport at the nanoscale with simple and robust model systems.

Gating has been successfully achieved in a number of man-made systems. Current rectification (*8*) and voltage-responsive pore opening (*9*–*11*) were demonstrated in polymer and solid-state nanopores having walls modified, for example, with single-stranded DNA (ssDNA), or polymer brushes. The transport properties of nanopores can also be made responsive to pressure (*12*–*14*), temperature (*15*), or molecules present in a solution, thus mimicking the behavior of ligand-gated channels (*2*, *16*–*18*).

The ability to efficiently transport one monovalent cation over another monovalent cation underpins key cellular processes such as signal propagation in neurons but is very challenging to achieve in artificial nanopores. One example includes anodic alumina membranes filled with silica that were rendered potassium selective via noncovalent attachment of crown ether (*19*). Graphene with crown ether–like nanopores was also proposed as a platform that could be made selective for a specific ion (*20*). In addition, the literature has shown a few examples of lipid bilayer–supported synthetic constructs prepared by supramolecular self-assembly to stack crown ether molecules on top of each other and create a channel (*21*–*25*). These synthetic pores, however, display only modest cation/cation selectivities. In a similar approach, self-assembly of rigid macrocycles formed hydrophobic nanopores in a lipid bilayer, which exhibited excellent selectivity toward protons over potassium ions and no measurable conductance in NaCl or LiCl (*26*). Because of their hydrophobic character, however, the macrocycle-based channels exhibited only very low, picosiemens conductivities in ionic strength as high as 4 M.

To our knowledge, cation/cation selectivity has not been reproduced yet in solid-state nanopores. This type of nanopore, which does not involve a lipid bilayer, offers the advantages of tunable geometry and surface properties and is far more robust than lipid bilayer–inserted channels. Thus, solid-state nanopores permit exploration into a wider range of electrochemical conditions and easier integration into fluidic devices.

Here, we demonstrate a solid-state nanopore that preferentially conducts potassium ions over sodium ions at concentrations up to 1 M and with selectivities far surpassing those previously reported in any other man-made nanopore platform. The mechanism of ionic selectivity is based on facilitated transport (*27*) of potassium ions through a nanopore with an effective opening of less than 2 nm, whose walls are decorated with 18-crown-6 ether molecules. In polar solvents such as water, this crown ether is known to selectively bind and release potassium ions quickly, allowing for their transport (*28*, *29*). We chose 4′-aminobenzo-18-crown-6 ether owing to the presence of an amino group that permits easy attachment to a carboxylated surface (*30*).

RESULTS AND DISCUSSION

Potassium selectivity is achieved via attachment of crown ether

Figure 1A shows the fabrication of single nanopores and the types of chemical modifications the structures were subjected to. The pores used in this study were formed in 30-nm-thick films of silicon nitride by dielectric breakdown (*31*–*33*). We measured transport characteristics of the as-prepared pores in 1 M and 100 mM solutions of KCl and NaCl (fig. S1). We then modified the pore walls and the membrane surfaces with triethoxysilylpropylmaleamic acid (TESPMA), which led

[1]Department of Physics and Astronomy, University of California, Irvine, Irvine, CA 92697, USA. [2]Department of Chemistry, Faculty of Engineering, Istanbul University Cerrahpasa, Avcılar-Istanbul, Turkey. [3]Lawrence Livermore National Laboratory, Livermore, CA 94550, USA. [4]Department of Chemistry, University of California, Irvine, Irvine, CA 92697, USA. [5]Department of Biomedical Engineering, University of California, Irvine, Irvine, CA 92697, USA.
*Corresponding author. Email: zsiwy@uci.edu (Z.S.S.); elifacar@istanbul.edu.tr (E.T.A.); buchsbaum1@llnl.gov (S.F.B.); fornasiero1@llnl.gov (F.F.)
†These authors contributed equally to this work.

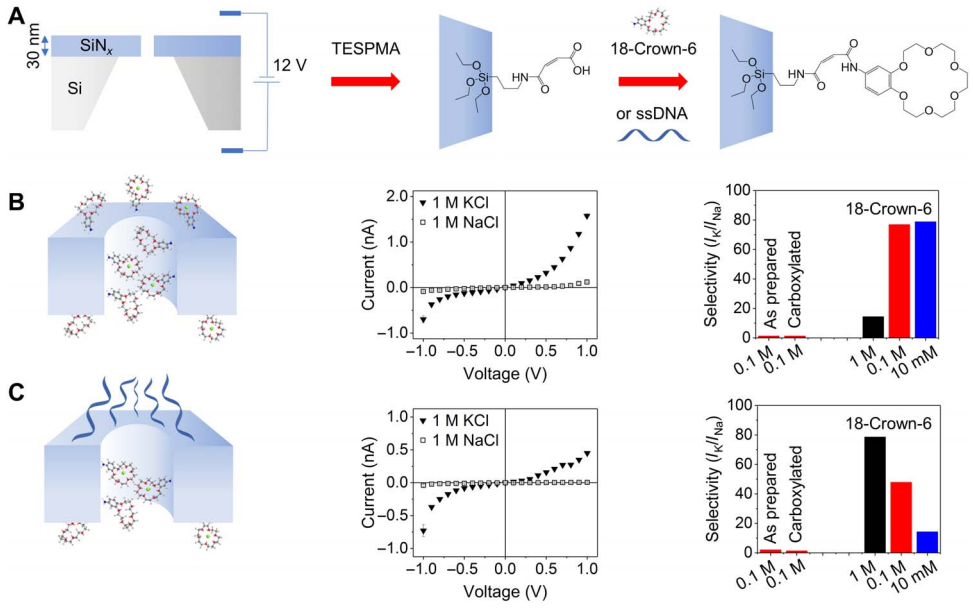

Fig. 1. Designing potassium-selective solid-state nanopores. (**A**) Single nanopores with a tunable opening diameter were created in 30-nm-thick silicon nitride films by the process of dielectric breakdown. The first modification step led to the attachment of carboxyl groups. The second modification involved either symmetric attachment of 4′-aminobenzo-18-crown-6 ether (B) or asymmetric modification with the crown ether and ssDNA (C). (**B**) *I-V* curves in 1 M KCl and 1 M NaCl recorded for a 1-nm-diameter pore whose walls were decorated with crown ether, as shown in the scheme. The graph on the right summarizes ratios of currents in KCl and NaCl at 1 V before and after each modification step for the same nanopore. Ratios of currents for the nanopore before and after carboxylation are calculated on the basis of the recordings in 100 mM of the salts. (**C**) *I-V* curves in 1 M KCl and 1 M NaCl for a 0.6-nm-wide nanopore modified with crown ether and ssDNA. Selectivity of the nanopore is shown as ratios of ionic currents in KCl and NaCl solutions measured under the same conditions as in (B).

to the attachment of carboxyl groups and the reduction of the pore diameter by a few nanometers (table S1) (*34*). Carboxylated nanopores were again tested in 1 M KCl and 100 mM KCl and NaCl solutions, and the pore resistance obtained from current-voltage (*I-V*) curves in 1 M solutions was used to size the pore diameter, assuming a cylindrical geometry (see the Supplementary Materials). All reported pore diameters in this work are therefore calculated after TESPMA functionalization. Because of possible deviation of the pores' shape from a cylinder, calculated diameters should be considered as average or effective diameters. Following carboxylation, nanopores were subjected to one of two modification strategies. (i) The first subset of nanopores (n = 3) was decorated with 4′-aminobenzo-18-crown-6 using 1-ethyl-3-(3-dimethylaminopropyl)carbodiimide (EDC) coupling chemistry (Fig. 1B) (*30*). (ii) The second subset of nanopores (n = 6) was modified from one side with ssDNA oligomer and from the other side with crown ether (Fig. 1C). This asymmetric functionalization scheme was motivated by the goal of combining voltage-gated transport and cation/cation selectivity in a single synthetic pore that mimics the structure and double functionality of potassium-gated channels (*6*, *7*). Reported selectivity of our pores toward potassium ions is defined here as the ratio of currents in KCl and NaCl solutions measured at 1 M, 100 mM, and 10 mM concentrations with a voltage of +1 V across the membrane. The positive sign of the electric potential difference corresponds to a working electrode on the side of the membrane with ssDNA; thus, for positive voltages, cations enter the pore from the DNA side and move toward the pore opening containing crown ether.

Figure 1B shows recordings for a 1-nm-wide nanopore modified with crown ether only. These include the ion selectivities before and after each modification step for all studied concentrations and the *I-V* curves in 1 M KCl and 1 M NaCl solutions. Selectivity toward potassium ions is evident only after attachment of crown ether so that the ionic current at +1 V in KCl solutions becomes at least 10 times higher than that in NaCl solutions. The pore shows current rectification; thus, the selectivity calculated at positive and negative voltages is different (fig. S2). Before implementing the asymmetric functionalization scheme (ii), we also tested the ionic selectivity of a pore subjected to crown modification only from one side. Current recordings for this pore (fig. S3) revealed that a partly modified pore still preferentially conducts potassium ions.

DNA plays the role of a cation filter

In our pore design inspired by voltage-gated ion channels, grafting of ssDNA was localized to the membrane surface and pore mouth through the selection of a 30-mer ssDNA, which is too large to diffuse inside the nanopore (*35*, *36*). We expected the high density of negative charges on the DNA to increase the cation concentrations at the pore entrance, thus causing the process of binding/releasing of ions from the crown ether to be the limiting step in the ion transport process. Note that potassium channels in a cell membrane also feature negative surface charges at one entrance, which are believed to increase local ionic concentrations and pore conductance (*7*). Example recordings for a 1-nm-wide pore subjected to ssDNA/crown ether modification are shown in Fig. 1C. In 1 M KCl, this pore exhibited potassium currents that were nearly 80 times higher than currents recorded in 1 M NaCl. Note that the potassium selectivity is induced by the presence of crown ether molecules; the highly charged DNA functions only as a cation filter, preventing anions from passing through (*37*). We believe that DNA does not contribute to the ability of the pore to distinguish between potassium and sodium ions, because a nanopore modified only with ssDNA exhibits comparable conductance in KCl and NaCl (fig. S4).

Potassium selectivity is based on facilitated transport

We hypothesized that the selectivity observed in the two nanopores shown in Fig. 1 is based on facilitated transport of K^+ ions (*27*), which undergo binding/unbinding to crown ether on the pore walls. In addition, we speculated that the effective pore opening after TESPMA (1 nm) is narrow enough to be fully occupied by the crown ether groups after EDC chemistry, thus preventing nonselective "bulk transport" of sodium ions through the middle section of the pore. Pore diameter is therefore predicted to play a very important role in determining the magnitude of K^+ selectivity.

Toward validating our hypothesis, we considered six ssDNA/crown ether–modified nanopores and three nanopores that contained only crown ether. In Fig. 2, we plotted the ratios of ionic currents recorded in KCl and NaCl solutions as a function of pore size determined after the carboxylation step. K^+ ion selectivity decreases exponentially with the increase in pore diameter and disappears for pore sizes larger than 3 nm. Thanks to the combined action of facilitated transport and negligible bulk transport, we could achieve K^+/Na^+ selectivities up to 84, which surpass those reported in other synthetic nanopores by about one order of magnitude. Note that pores with effective diameter below 1 nm could have been too narrow to allow for the attachment of crown ether along the pore length. In the case of very narrow pores, the chemical modification could be restricted mostly to the membrane surface/pore entrance, which was sufficient to render the nanopores potassium ion selective.

Another notable finding is the increase in K^+ selectivity with salt concentration for the majority of nanopores with a diameter of less than 2 nm, a dependence that contradicts expectations from an electrostatics-based selectivity mechanism. To understand this observation, we looked in detail at the concentration dependence of sodium and potassium currents (Fig. 3 and fig. S5). Sodium currents in <2-nm nanopores are nearly concentration independent, which suggests that the nanopores are too small to allow for significant nonselective transport of sodium through the pore middle region. Potassium currents on the other hand do depend on the bulk concentration; thus, the ratio of currents in potassium and sodium is lower at lower concentrations.

Figure 2 also offers comparison between pores modified only with crown ether and those with both DNA and crown ether functionalities. Although both types of nanopores can exhibit ratios of currents in KCl and NaCl solutions >78, the pores modified only with crown ether lose their selectivity more rapidly with the increase in pore size. This observation supports our prediction that DNA would act as a cation selectivity filter and/or contribute to further narrow the size of any nonselective transport pathway at the pore center. Overall, our finding suggests a larger robustness of the potassium selectivity in the presence of DNA.

Similar to the pores modified only with crown ether, pores functionalized with both ssDNA and crown ether displayed current rectification and different selectivities with voltage sign. The difference in K^+/Na^+ selectivity between positive and negative voltages can be explained, considering that crown ether acquires a positive charge in the presence of cations (*37*). Consequently, a DNA/crown ether nanopore system features oppositely charged membrane surfaces, which can give rise to a diode behavior (*8*). Continuum modeling with the Poisson-Nernst-Planck equations shows that for positive voltages, ionic concentrations in the pore are higher and that the electric potential decays nearly linearly across the entire pore length (figs. S6 and S7). Negative voltages, on the other hand, cause the formation of a depletion zone with a localized voltage drop. Thus, the resulting weak voltage gradient in the crown ether–modified region induces a smaller selectivity.

Last, we looked at the voltage dependence of potassium ion selectivity. All pores examined exhibited a selectivity increase at larger positive voltages, the magnitude of which is strongly dependent on pore size (Fig. 3). The sensitivity of selectivity to voltage was maximized at a pore diameter of ~1 nm and decreased for both larger and smaller pores.

Selectivity of DNA/crown ether–modified nanopores in KCl and NaCl mixtures

We performed the measurements shown above with only one type of salt present in solution. We therefore designed additional experiments to test the performance of the K^+-selective nanopores in mixtures of two salts, KCl and NaCl. We performed the current recordings in solutions in which the total concentration of cations was kept at a constant level of 1 M. The following mixtures were studied: 0.8 M KCl + 0.2 M NaCl, 0.7 M KCl + 0.3 M NaCl, and 0.5 M KCl + 0.5 M NaCl. In addition, we performed measurements in 1 M KCl and 1 M NaCl. Figure 4 and fig. S8 show *I-V* curves obtained in mixtures and in individual salts together with the magnitudes of the current at +1 V as a function of KCl concentration. The pore examined had an effective opening diameter of 1 nm and was modified with crown ether and DNA. To calculate selectivity of the nanopore in salt mixtures,

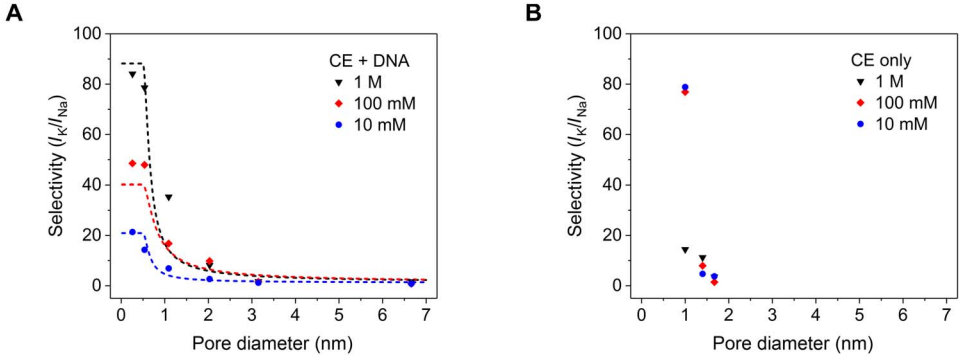

Fig. 2. Selectivity of nanopores toward potassium. (**A**) Experimental ratios of ion currents in KCl and NaCl solutions for six independently prepared nanopores subjected to chemical modification with crown ether (CE) and ssDNA. Data for three different bulk concentrations of the salts are shown. The model fit is shown as dashed lines. (**B**) Experimental data of potassium selectivity for three nanopores modified only with crown ether. SDs of currents for individual voltages are shown in *I-V* curves in Fig. 1 and fig. S5.

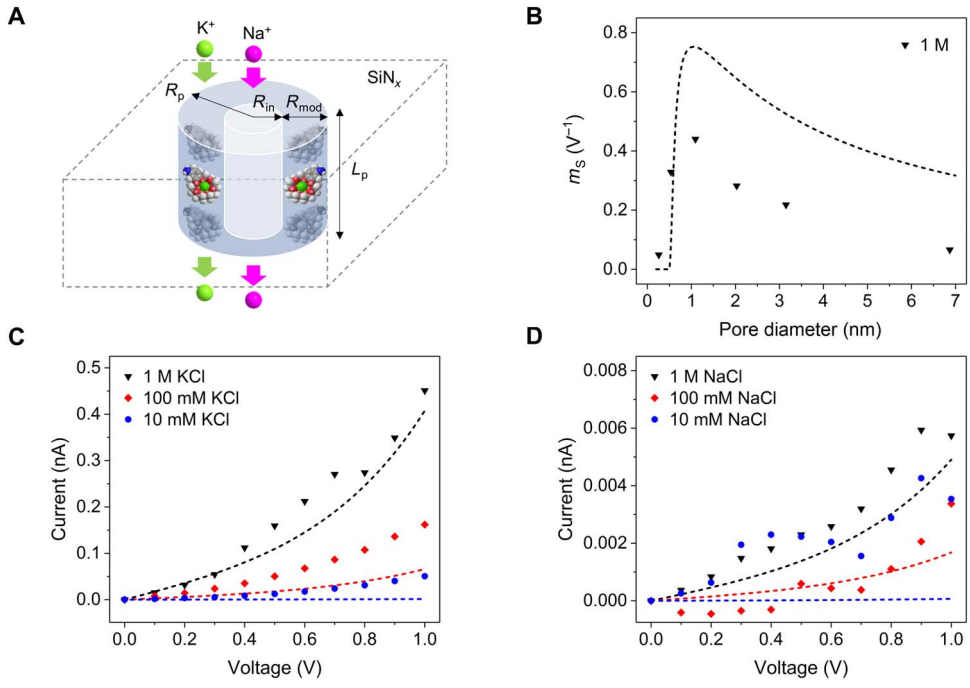

Fig. 3. Phenomenological model of the potassium selectivity of solid-state nanopores. (**A**) Scheme of the modeled system with geometrical parameters used in the model. (**B**) Diameter dependence of the selectivity sensitivity (m_S) to voltage. m_S is defined here as the slope of a linear fit of $\log(I_K/I_{Na})$ versus voltage for 1 M KCl and NaCl solution concentrations. (**C**) *I-V* curves at three different bulk KCl concentrations for the same pore shown in Fig. 1C. (**D**) *I-V* curves at three different bulk NaCl concentrations for the same pore as (C). Symbols are for experimental data, while dashed lines represent model predictions using the parameters listed in Table 1. SDs of currents for individual voltages are shown in *I-V* curves in fig. S5.

we recalled that sodium currents did not depend on NaCl concentration in the range between 10 mM and 1 M (fig. S5). Selectivity can then be obtained as a ratio of the current observed in a given mixture and the current magnitude recorded in 1 M NaCl. Our measurements revealed that although selectivity dropped from ~20 in 1 M KCl to ~5 in 0.8 M KCl and 0.2 M NaCl, the pore remained selective when the salts were present at equal concentrations (0.5 M). Recorded ionic currents dropped proportionally to the selectivity change upon addition of sodium ions.

Phenomenological model with voltage-dependent k_{on} and k_{off} helps explain potassium selectivity of nanopores

Toward validating the claim that the pore behavior discussed thus far can be explained by crown ether–mediated transport, we developed a simple model, which neglects the presence of DNA and any surface charge effects. We assumed a pore with walls decorated by crown ether arranged in a ring, which interacts with cations through binding/unbinding events governed by k_{on} and k_{off} rate constants. For simplicity, we focused only on transport through a single crown ether layer (Fig. 3A). Both k_{on} and k_{off} constants depend exponentially on voltage, V, according to $k_i = k_{i0}e^{-\frac{d_{ce}eV}{L_p k_B T}}$, i = on, off, where $\frac{d_{ce}}{L_p}$ corresponds to the fractional potential drop an ion experiences as it approaches and binds to a crown ether, L_p is the pore length, e is the unit charge, and k_B is the Boltzmann constant (*18*, *38*, *39*). The total current in the crown ether region can then be calculated from the total time, τ, an ion takes to pass through the pore, $\tau = \frac{1}{k_{on}C} + \frac{1}{k_{off}}$, the charge density calculated from the percentage of bound cation/crown ether complexes, the ion concentration C, and the pore radius R_p. To approximate a leakage current, the model assumes bulk transport in the center of the pore if $R_p > R_{mod}$, where R_{mod} is the constant radial thickness of the crown ether–modified region. We set the pore length L_p equal to 30 nm to match the experimental system. The model was then fit to the combined experimental dataset of *I-V* for the nanopore shown in Fig. 1C and selectivity versus pore diameter for all ssDNA/crown ether–modified pores (Fig. 2A) while keeping R_{mod} constant at 0.25 nm. Best-fit values of parameters are summarized in Table 1. Fitted d_{ce} suggests a reasonable spacing between crown ethers of 1 nm to a few nanometers, while the binding constants, especially for K^+, differ significantly from those seen in a bulk system (*28*). While at first unexpected, this result appears to be supported by previously reported theories that binding/unbinding kinetics of close-packed macrocycles under nanoscale confinement can deviate substantially from bulk behavior (*22*, *23*).

The model is able to successfully capture several key trends observed in the experimental data, the first of which is the diameter dependence of selectivity versus pore diameter (Fig. 2A). As expected, the selectivity decreases for large pores due to leakage current while plateauing at a maximum for small pore diameters, where the leakage current becomes negligible. Next, the model reproduces well the exponential current dependence on voltage along with reasonably accurate current magnitudes (Fig. 3, C and D). Our set of equations also replicates the experimentally observed weaker concentration dependence for NaCl versus KCl current, which we attribute to Na^+ transport being limited by the concentration-independent k_{off}. In addition, the model portrays how the voltage dependence of the K^+/Na^+ selectivity changes with pore diameter (Fig. 3D). At small enough pore size, the leakage current drops to zero, and the selectivity becomes voltage

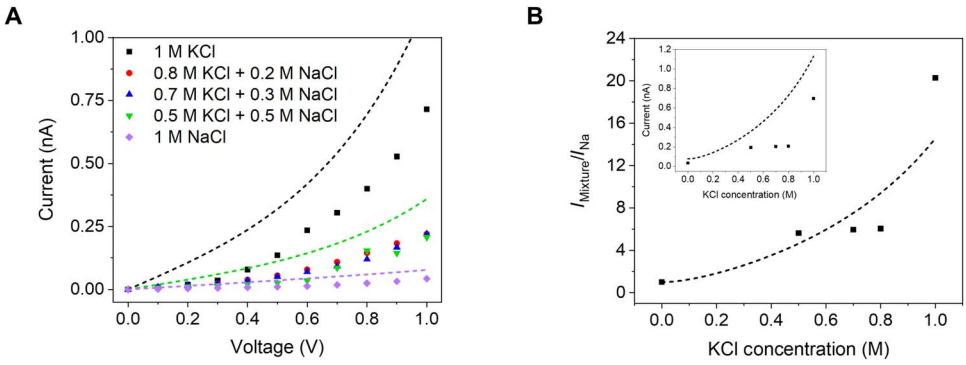

Fig. 4. Ion current measurements in mixtures of KCl and NaCl for a 1-nm-diameter nanopore modified with crown ether and DNA. (**A**) *I-V* curves in all conditions examined. (**B**) Ratio of the ionic currents in mixed salt solutions and in 1 M NaCl solution as a function of KCl concentration at +1 V and a constant total salt concentration of 1 M. The inset shows the magnitude of the ion current as a function of KCl concentration under the same conditions. Dashed lines show model predictions using the parameters given in Table 1 for a 1-nm-diameter pore.

Table 1. Values of parameters used to fit the experimental data of potassium selectivity and ion current values (Figs. 2 to 4).

$k_{off0,K}$ (s^{-1})	$k_{on0,K}$ (s^{-1} M^{-1})	$\frac{k_{on0,K}}{k_{off0,K}}$ (M)	$k_{off0,Na}$ (s^{-1})	$k_{on0,Na}$ (s^{-1} M^{-1})	$\frac{k_{on0,Na}}{k_{off0,Na}}$ (M)	d_{ce} (nm)
9.9×10^8	5.1×10^9	5.15	9.2×10^6	1.1×10^8	11.95	1.9

independent since both K^+ and Na^+ binding rates respond to voltage similarly. As the pore diameter becomes too large, the leakage current begins to dominate, and thus, the selectivity becomes less sensitive to voltage.

Last, our phenomenological model explains the decrease in ionic current and selectivity when sodium ions are added to a potassium chloride solution. Since the absorption equilibrium constant k_{on}/k_{off} for Na^+ is larger than that for K^+ ions and $k_{off,Na}$ is two orders of magnitude lower than $k_{off,K}$, a large fraction of the crown ether is occupied by tightly bound sodium ions rather than efficiently transporting fast-releasing potassium ions. Thus, competitive binding of sodium slows down potassium transport. Overall, the ability of this simple model to reproduce all observed trends in the data strongly supports the proposed facilitated transport mechanism, and this simple set of equations may prove to be useful in the design of future biomimetic pores.

CONCLUSIONS

In conclusion, we presented a solid-state nanopore system decorated with crown ether, which renders the pores highly selective toward potassium ions when the pore diameter is sufficiently small. We found that placement of ssDNA at one pore entrance made the system selectivity more robust by concentrating cations at one entrance. Future studies will focus on equipping such a potassium-selective pore with a voltage-gated component to enable voltage-regulated pore opening. We will also identify experimental conditions and different types of crown ethers, which may offer highly efficient potassium ion transport even in salt mixtures.

MATERIALS AND METHODS

Preparation of nanopores

Single nanopores were prepared by the process of dielectric breakdown (*31*–*33*) in low-stress silicon nitride (SiN_x) membranes (50 μm by 50 μm; thickness, 30 nm) purchased from Norcada. Before the pore fabrication, the chips were washed in piranha solution (H_2O_2:H_2SO_4, 1:3) at 100°C for 30 min, followed by rinsing in 18-megohm water.

In the dielectric breakdown process, both chambers of a custom-made polydimethylsiloxane conductivity cell were filled with a strongly acidic solution of 1 M KCl (pH 1.6) (*32*, *33*). The dielectric breakdown was performed with 12 V applied with two Ag/AgCl pellet electrodes. The electric field chosen (0.4 V/nm) is close to the minimum magnitude needed to create nanopores by this technique, which assures formation of one pore only (*31*, *40*). The pore formed after ~60 min; the process was stopped after the current increased by ~100 nA above the baseline current. The pore diameter was estimated on the basis of the pore resistance found from the *I-V* curve recorded in 1 M KCl in the voltage range between −1 and +1 V. Note that the total resistance is a sum of the geometrical pore resistance and access resistance (*41*). The opening diameter (*D*) was then estimated using the following equation (*33*)

$$D = \frac{G}{2\sigma}\left[1 + \sqrt{1 + \frac{16\sigma L}{\pi G}}\right] \quad (1)$$

where *G* is the slope of the *I-V* curve, σ stands for the solution conductivity, and *L* is the pore length (30 nm). The shape of the pores was assumed cylindrical; thus, the calculated diameters are considered effective/average diameters.

I-V curves were measured with Axopatch 200B and Digidata 1322A (Molecular Devices Inc.) using a sampling frequency of 10 kHz with 0.1-V voltage steps. At each voltage step, the current signal was recorded for 100 s. The current values reported are averages of the whole time series except for the first and last 5 s of the recordings. Two pellet Ag/AgCl electrodes were used for all current measurements.

Modification of nanopores with TESPMA

The modification solution was prepared by adding 50 mg of TESPMA to 5 ml of ultrapure water containing acetic acid (50 μl); the solution was stirred for 1 hour at room temperature. Nanopore silicon nitride chips were immersed in the solution at room temperature for 1 hour. After washing in deionized water, the chips were heated at 80°C for 20 min (*34*). TESPMA-modified nanopores were resized in 1 M KCl using the same procedure as described above.

Attachment of crown ether and DNA

After carboxylation, silicon nitride chips were subjected to chemical modification with 4-aminobenzo-18-crown-6 (4-AB18C6) crown ether and DNA. Both molecules were attached using EDC-mediated chemistry to link amino groups to carboxyls. To this end, silicon nitride nanopore chips were first activated from both sides using a solution of 0.01 M EDC and 0.02 M *N*-hydroxysulfosuccinimide in 0.1 M MES buffer (pH 5.5). The activation time was kept constant at 30 min, which was followed by a thorough wash of the membrane with 0.1 M MES buffer solution from both sides. Attachment of crown ether molecules was performed overnight by incubation of the chips in a solution of 0.01 M 4-AB18C6 in 0.1 M MES buffer (pH 5.5) (*37*). One nanopore was modified with the crown ether asymmetrically; this modification was performed in a conductivity cell so that one chamber of the cell contained the crown ether solution, while the other side contained only 0.1 M MES buffer (pH 5.5); the asymmetric modification was expected to result in the attachment of the molecules only to about a half of the pore length.

DNA oligomer of the following sequence was purchased from Integrated DNA Technologies (Coralville, IA): 5′-/5AmMC12/CACCCACAACCACCAACACACACCACCACC-3′. The amino group with a linker was shown before to allow attachment of DNA oligomers to carboxylated surfaces (*9*). An amount of oligomer was dissolved in 0.1 M MES buffer (pH 5.5) to reach a DNA concentration of ~0.5 mM. All DNA modifications were performed in a conductivity cell. One side of the chip was in contact with the DNA solution, and the other side was in contact with the solution of crown ether. The reaction occurred overnight. Properties of DNA and 4-AB18C6–modified nanopores were examined in KCl solutions buffered to pH 8.

SUPPLEMENTARY MATERIALS

Supplementary material for this article is available at http://advances.sciencemag.org/cgi/content/full/5/2/eaav2568/DC1

Fig. S1. Examples of *I-V* curves for the nanopores shown in Fig. 1 before crown ether attachment.

Fig. S2. Selectivity of nanopores shown in Fig. 1 toward potassium ions at −1 V.

Fig. S3. Ion selectivity at 1 V of a nanopore modified with crown ether from one side only.

Fig. S4. Ion current through a 1-nm-diameter nanopore modified with DNA from one side.

Fig. S5. Ion currents through a nanopore shown in Fig. 1C as a function of KCl and NaCl concentrations.

Fig. S6. Scheme of a modeling system used to predict local ionic concentrations and electric potential in a nanopore.

Fig. S7. Results of numerical modeling of ionic concentrations and electric potential in a nanopore shown in fig. S6.

Fig. S8. *I-V* curves for the nanopore shown in Fig. 4.

Table S1. Pore opening diameters calculated according to Eq. 1 for all nanopores considered in the manuscript.

REFERENCES AND NOTES

1. M. Barboiu, A. Gilles, From natural to bioassisted and biomimetic artificial water channel systems. *Acc. Chem. Res.* **46**, 2814–2823 (2013).
2. X. Hou, W. Guo, L. Jiang, Biomimetic smart nanopores and nanochannels. *Chem. Soc. Rev.* **40**, 2385–2401 (2011).
3. S. W. Kowalczyk, T. R. Blosser, C. Dekker, Biomimetic nanopores: Learning from and about nature. *Trends Biotechnol.* **29**, 607–614 (2011).
4. M. Tagliazucchi, I. Szleifer, Transport mechanisms in nanopores and nanochannels: Can we mimic nature? *Mater. Today* **18**, 131–142 (2015).
5. B. Hille, *Ion Channels of Excitable Membranes* (Oxford Univ. Press, 2001).
6. R. MacKinnon, Potassium channels and the atomic basis of selective ion conduction (Nobel lecture). *Angew. Chem. Int. Ed. Engl.* **43**, 4265–4277 (2004).
7. D. A. Doyle, J. M. Cabral, R. A. Pfuetzner, A. Kuo, J. M. Gulbis, S. L. Cohen, B. T. Chait, R. MacKinnon, The structure of the potassium channel: Molecular basis of K^+ conduction and selectivity. *Science* **280**, 69–77 (1998).
8. Z. S. Siwy, S. Howorka, Engineered voltage-responsive nanopores. *Chem. Soc. Rev.* **39**, 1115–1132 (2010).
9. S. F. Buchsbaum, G. Nguyen, S. Howorka, Z. S. Siwy, DNA-modified polymer pores allow pH- and voltage-gated control of channel flux. *J. Am. Chem. Soc.* **136**, 9902–9905 (2014).
10. C. C. Harrell, P. Kohli, Z. Siwy, C. R. Martin, DNA–nanotube artificial ion channels. *J. Am. Chem. Soc.* **126**, 15646–15647 (2004).
11. F. Xia, W. Guo, Y. Mao, X. Hou, J. Xue, H. Xia, L. Wang, Y. Song, H. Ji, Q. Ouyang, Y. Wang, L. Jiang, Gating of single synthetic nanopores by proton-driven DNA molecular motors. *J. Am. Chem. Soc.* **130**, 8345–8350 (2008).
12. S. N. Smirnov, I. V. Vlassiouk, N. V. Lavrik, Voltage-gated hydrophobic nanopores. *ACS Nano* **5**, 7453–7461 (2011).
13. M. R. Powell, L. Cleary, M. Davenport, K. J. Shea, Z. S. Siwy, Electric-field-induced wetting and dewetting in single hydrophobic nanopores. *Nat. Nanotechnol.* **6**, 798–802 (2011).
14. J. L. Trick, P. Aryal, S. J. Tucker, M. S. P. Sansom, Molecular simulation studies of hydrophobic gating in nanopores and ion channels. *Biochem. Soc. Trans.* **43**, 146–150 (2015).
15. M. Gopinadhan, P. Deshmukh, Y. Choo, P. W. Majewski, O. Bakajin, M. Elimelech, R. M. Kasi, C. O. Osuji, Thermally switchable aligned nanopores by magnetic-field directed self-assembly of block copolymers. *Adv. Mater.* **26**, 5148–5154 (2014).
16. Z. Siwy, L. Trofin, P. Kohli, L. A. Baker, C. Trautmann, C. R. Martin, Protein biosensors based on biofunctionalized conical gold nanotubes. *J. Am. Chem. Soc.* **127**, 5000–5001 (2005).
17. H. Zhang, Y. Tian, L. Jiang, Fundamental studies and practical applications of bio-inspired smart solid-state nanopores and nanochannels. *Nano Today* **11**, 61–81 (2016).
18. R. Wei, V. Gatterdam, R. Wieneke, R. Tampé, U. Rant, Stochastic sensing of proteins with receptor-modified solid-state nanopores. *Nat. Nanotechnol.* **7**, 257–263 (2012).
19. A. Cazacu, Y.-M. Legrand, A. Pasc, G. Nasr, A. Van der Lee, E. Mahon, M. Barboiu, Dynamic hybrid materials for constitutional self-instructed membranes. *Proc. Natl. Acad. Sci. U.S.A.* **106**, 8117–8122 (2009).
20. J. Guo, J. Lee, C. I. Contescu, N. C. Gallego, S. T. Pantelides, S. J. Pennycook, B. A. Moyer, M. F. Chisholm, Crown ethers in graphene. *Nat. Commun.* **5**, 5389 (2014).
21. A. J. Wright, S. E. Matthews, W. B. Fischer, P. D. Beer, Novel resorcin[4]arenes as potassium-selective ion-channel and transporter mimics. *Chem. Eur. J.* **7**, 3474–3481 (2001).
22. Z. H. Sun, M. Barboiu, Y.-M. Legrand, E. Petit, A. Rotaru, Highly selective artificial cholesteryl crown ether K^+-channels. *Angew. Chem. Int. Ed. Engl.* **54**, 14473–14477 (2015).
23. C. Ren, J. Shen, H. Zeng, Combinatorial evolution of fast-conducting highly selective K^+-channels via modularly tunable directional assembly of crown ethers. *J. Am. Chem. Soc.* **139**, 12338–12341 (2017).
24. A. Gilles, M. Barboiu, Highly selective artificial K^+ channels: An example of selectivity-induced transmembrane potential. *J. Am. Chem. Soc.* **138**, 426–432 (2016).
25. W. X. Feng, Z. Sun, Y. Zhang, Y.-M. Legrand, E. Petit, C.-Y. Su, M. Barboiu, Bis-15-crown-5-ether-pillar[5]arene K^+-responsive channels. *Org. Lett.* **19**, 1438–1441 (2017).
26. X. B. Zhou, G. Liu, K. Yamato, Y. Shen, R. Cheng, X. Wei, W. Bai, Y. Gao, H. Li, Y. Liu, F. Liu, D. M. Czajkowsky, J. Wang, M. J. Dabney, Z. Cai, J. Hu, F. V. Bright, L. He, X. C. Zeng, Z. Shao, B. Gong, Self-assembling subnanometer pores with unusual mass-transport properties. *Nat. Commun.* **3**, 949 (2012).
27. P. H. von hippel, O. G. Berg, Facilitated target location in biological systems. *J. Biol. Chem.* **264**, 675–678 (1989).
28. R. M. Izatt, J. S. Bradshaw, S. A. Nielsen, J. D. Lamb, J. J. Christensen, D. Sen, Thermodynamic and kinetic data for cation-macrocycle interaction. *Chem. Rev.* **85**, 271–339 (1985).
29. R. M. Izatt, K. Pawlak, J. S. Bradshaw, R. L. Bruening, Thermodynamic and kinetic data for macrocycle interaction with cations, anions, and neutral molecules. *Chem. Rev.* **95**, 2529–2586 (1995).
30. G. T. Hermanson, *Bioconjugate Techniques* (Academic Press, ed. 3, 2013).
31. H. Kwok, K. Briggs, V. Tabard-Cossa, Nanopore fabrication by controlled dielectric breakdown. *PLOS ONE* **9**, e92880 (2014).
32. I. Yanagi, K. Fujisaki, H. Hamamura, K.-i. Takeda, Thickness-dependent dielectric breakdown and nanopore creation on sub-10-nm-thick SiN membranes in solution. *J. Appl. Phys.* **121**, 045301 (2017).
33. E. T. Acar, P. Hinkle, Z. S. Siwy, Concentration-polarization-induced precipitation and ionic current oscillations with tunable frequency. *J. Phys. Chem. C* **122**, 3648–3654 (2018).
34. Y. Kurihara, M. Takama, T. Sekiya, Y. Yoshihara, T. Ooya, T. Takeuchi, Fabrication of carboxylated silicon nitride sensor chips for detection of antigen–antibody reaction using microfluidic reflectometric interference spectroscopy. *Langmuir* **28**, 13609–13615 (2012).
35. A. Y. L. Sim, J. Lipfert, D. Herschlag, S. Doniach, Salt dependence of the radius of gyration and flexibility of single-stranded DNA in solution probed by small-angle x-ray scattering. *Phys. Rev. E* **86**, 021901 (2012).

36. P. G. de Gennes, *Scaling Concepts in Polymer Physics* (Cornell Univ. Press, 1979).
37. G. Pérez-Mitta, A. G. Albesa, W. Knoll, C. Trautmann, M. E. Toimil-Molares, O. Azzaroni, Host–guest supramolecular chemistry in solid-state nanopores: Potassium-driven modulation of ionic transport in nanofluidic diodes. *Nanoscale* **7**, 15594–15598 (2015).
38. B. Hornblower, A. Coombs, R. D. Whitaker, A. Kolomeisky, S. J. Picone, A. Meller, M. Akeson, Single-molecule analysis of DNA-protein complexes using nanopores. *Nat. Methods* **4**, 315–317 (2007).
39. A. M. Woodhull, Ionic blockage of sodium channels in nerve. *J. Gen. Physiol.* **61**, 687–708 (1973).
40. Y. Wang, C. Ying, W. Zhou, L. de Vreede, Z. Liu, J. Tian, Fabrication of multiple nanopores in a SiN_x membrane via controlled breakdown. *Sci. Rep.* **8**, 1234 (2018).
41. J. E. Hall, Access resistance of a small circular pore. *J. Gen. Physiol.* **66**, 531–532 (1975).

Acknowledgments: We are grateful to M. S. P. Sansom and S. J. Tucker from the University of Oxford for discussions. **Funding:** This work was funded by NSF (CBET-1803262) and by the Scientific and Technological Research Council of Turkey (TUBITAK), 2219-International Postdoctoral Research Fellowship Program (application no. 1059B191600613). E.T.A. also acknowledges the Istanbul University Cerrahpasa, Engineering Faculty Chemistry Department for additional financial support. E.T.A., S.F.B., and F.F. acknowledge support from the Laboratory Directed Research and Development Program at LLNL under project tracking code 18-LW-057. Work at LLNL was performed under the auspices of the U.S. Department of Energy under contract DE-AC52-07NA27344. **Author contributions:** E.T.A. collected experimental results, analyzed the results, and wrote the manuscript. S.F.B. developed the phenomenological model and wrote the manuscript. C.C. performed numerical modeling. F.F. analyzed the data, developed the phenomenological model, and wrote the manuscript. Z.S.S. designed the experiments, analyzed the data, and wrote the manuscript.
Competing interests: The authors declare that they have no competing interests.
Data and materials availability: All data needed to evaluate the conclusions in the paper are present in the paper and/or the Supplementary Materials. They can be obtained by contacting the authors. Additional data related to this paper may be requested from the authors.

Submitted 29 August 2018
Accepted 21 December 2018
Published 8 February 2019
10.1126/sciadv.aav2568

Citation: E. T. Acar, S. F. Buchsbaum, C. Combs, F. Fornasiero, Z. S. Siwy, Biomimetic potassium-selective nanopores. *Sci. Adv.* **5**, eaav2568 (2019).

ScienceAdvances

Biomimetic potassium-selective nanopores

Elif Turker Acar, Steven F. Buchsbaum, Cody Combs, Francesco Fornasiero and Zuzanna S. Siwy

Sci Adv **5** (2), eaav2568.
DOI: 10.1126/sciadv.aav2568